NRC Research Press

ARTICLE

Modeling the nonlinear elastic behavior of plant epidermis[1]

Amir J. Bidhendi, Hongbo Li, and Anja Geitmann

Abstract: Cell growth and organ development in plants are often correlated with the tensile behavior of the primary cell wall. To understand the mechanical behavior of plant material, various mechanical testing techniques have been employed, such as tensile testing of excised tissue samples. The onion (*Allium cepa* L.) epidermis has emerged as a model system for plant tissue mechanics. In this study, we performed tensile tests on strips of adaxial onion epidermis. While the tissue appeared stiffer in the direction along the major growth axis compared with the transverse direction, the tensile strength of tissue was not significantly different between the two orientations, indicating a nontrivial link between the cell wall and tissue mechanical anisotropy. Importantly, we observed the stress–strain behavior of the onion epidermis under tension to be highly nonlinear. Several hyperelastic models were fitted to the test data to evaluate their capacity to describe the nonlinear deformation of onion epidermis. The Yeoh hyperelastic model could successfully simulate the uniaxial tensile test data. This study suggests that accounting for nonlinearity in the deformation of the primary tissue may be essential for the accurate interpretation of mechanical test data, and a better understanding of the mechanics of the primary plant cell wall.

Key words: epidermis, plant cell mechanics, nonlinear elasticity, hyperelasticity, uniaxial tensile testing, finite element analysis.

Résumé : La croissance cellulaire et le développement des organes chez les plantes sont souvent corrélés au comportement en traction de la paroi cellulaire primaire. Afin de comprendre le comportement mécanique de la matière végétale, plusieurs tests mécaniques ont été réalisés, tels que l'essai de traction sur des échantillons de tissus excisés. L'épiderme de l'oignon (*Allium cepa* L.) est apparu comme un système modèle de la mécanique des tissus végétaux. Dans cette étude, les auteurs ont réalisé des essais de traction sur des bandes d'épiderme adaxial de l'oignon. Alors que le tissu semblait plus rigide le long de l'axe principal de croissance comparativement au sens transverse, les forces de traction du tissu n'étaient pas significativement différentes entre les deux orientations, indiquant l'existence d'un lien non négligeable entre la paroi cellulaire et l'anisotropie mécanique du tissu. Fait à noter, ils ont observé que le comportement de contrainte-déformation de l'épiderme de l'oignon placé sous tension était hautement non linéaire. Plusieurs modèles hyperélastiques ont été apposés aux données expérimentales afin d'évaluer leur capacité à décrire la déformation non linéaire de l'épiderme de l'oignon. Le modèle hyperélastique de Yeoh pouvait simuler avec succès les données de l'essai de traction uniaxiale. Cette étude suggère que la prise en compte de la non-linéarité de la déformation du tissu primaire peut être essentielle à l'interprétation exacte des données d'essais mécaniques et à une meilleure compréhension de la mécanique de la paroi cellulaire primaire des plantes. [Traduit par la Rédaction]

Mots-clés : épiderme, mécanique des cellules végétales, élasticité non linéaire, hyperélasticité, essai de traction uniaxiale, analyse par éléments finis.

Introduction

Cell walls are composite materials that encapsulate the plant protoplast. Growing plant cells are characterized by primary cell walls that accommodate cell expansion. The chemical composition and mechanical properties of the primary plant cell walls are correlated with a host of plant activities such as sperm delivery and fertilization, organogenesis, cell-level morphogenesis, and plant defense (Cosgrove 2005; Osorio et al. 2008; Fayant et al. 2010; Kierzkowski et al. 2012; Braybrook and Peaucelle

Received 11 March 2019. Accepted 6 July 2019.

A.J. Bidhendi and A. Geitmann.* Department of Plant Science, McGill University, Macdonald Campus, 21111 Lakeshore, Ste-Anne-de-Bellevue, QC H9X 3V9, Canada.
H. Li. College of Engineering, Shanxi Agricultural University, Taigu, Shanxi 030801, P.R. China.
Corresponding author: Anja Geitmann (email: geitmann.aes@mcgill.ca).
*Anja Geitmann currently serves as a Guest Editor; peer review and editorial decisions regarding this manuscript were handled by Christian Lacroix.
[1]This Article is part of a Special Issue from the 9th International Plant Biomechanics Conference (9–14 August 2018, McGill University).

2013; Bidhendi and Geitmann 2016; Phyo et al. 2017; Bidhendi and Geitmann 2018*a*; Cosgrove 2018; Sapala et al. 2018; Bidhendi et al. 2019). During cell growth, the hydrostatic pressure within the cell and the uptake of water are thought to drive irreversible wall expansion following the biochemical modulation of the cell wall. Morphogenetic processes such as directional growth are attributed to mechanical anisotropy and heterogeneity of the cell wall (Cosgrove 2015; Bidhendi and Geitmann 2016). Various mechanical testing techniques are used to quantify and correlate the mechanical properties of the cell wall with cell and organ morphogenesis. Mechanical testing techniques such as nanoindentation or tensile testing have been used to characterize plant material at the tissue or subcellular level, and their application has been critically reviewed (Milani et al. 2013; Bidhendi and Geitmann 2019). The outcome of the mechanical assessment of plant cells and tissues has led to insight on cell-growth-related features such as mechanical anisotropy of the cell wall and enzymatic activity. Many studies have attempted to correlate the subcellular mechanical behavior of the cell wall with cell growth (Bolduc et al. 2006; Fayant et al. 2010; Sanati Nezhad et al. 2013; Carter et al. 2017) or, at a larger scale, with tissue growth and organogenesis (Braybrook and Peaucelle 2013; Peaucelle et al. 2015; Bou Daher et al. 2018). Experimental strategies to study the mechanics of primary plant cells and tissue mostly rely on the application of some type of force and examining the response of the tissue. However, how the results obtained by some of these techniques correlate with in-plane mechanical properties of the cell wall — those that are thought to be directly relevant for the cell wall's resistance to turgor driven expansion, is sometimes convoluted (Braybrook and Peaucelle 2013; Bidhendi and Geitmann 2019).

Tension tests are among the techniques widely used to characterize biological materials. Unlike techniques involving complex loading conditions such as indentation-based methods, loading in tensile testing may be more easily reconcilable with in-plane tension of the cell wall under turgor. Tensile testing on plant material has mostly been performed at tissue-scale, regardless of the scale to which the findings were attributed (Ryden et al. 2003; Vanstreels et al. 2005; Suslov and Verbelen 2006; Oey et al. 2007; Saxe et al. 2016). This is generally due to technical challenges associated with sample preparation and testing at miniature scales. As a result, except for a few studies that carried out tensile tests on cell wall fragments (Toole et al. 2001; Wei et al. 2006; Zamil et al. 2013, 2015), tensile testing has remained limited to tissue scale tests. In uniaxial tensile testing, the sample is gripped and stretched in one direction while the force required to stretch the sample is registered. This information is used to calculate the stress–strain relationships and consequently the material parameters, such as Young's modulus quantifying the resistance of the plant material against deformation (Bidhendi and Geitmann 2018*b*).

The onion epidermis has emerged as a model in a wide range of studies involving the study of plant tissue and cell mechanics. Studies investigating the effect of enzymes, or polymer interactions in the cell wall network, the tensile behavior of plant material, or bio-inspired design have benefited from the use of onion epidermis (Vanstreels et al. 2005; Suslov and Verbelen 2006; Van Sandt et al. 2007; Suslov et al. 2009; Zamil et al. 2013; Chen et al. 2015; Kim et al. 2015; Zhang et al. 2016). A set of desirable properties render the onion epidermis a suitable specimen for such studies. For instance, the adaxial onion epidermis is readily detachable from the underlying layers providing intact plant tissue specimens that are a single cell thick. The abaxial onion epidermis, on the other hand, often rips open upon detachment, which allows us to study the composition of the most recently synthesized wall layers at inner faces of the cell walls using techniques such as atomic force microscopy (Zhang et al. 2016). Another important property of the onion epidermis is the fairly regular, brick-like shape of its cells and the simple alignment of their major growth axes with respect to the onion bulb axis. The simple geometry of onion epidermal cells simplifies, at least to some degree, the investigation of the effect of cellular shape and arrangement on tissue-level mechanical properties as it reduces the confounding cell geometrical variabilities.

A few studies have investigated the tensile properties of the onion epidermis (Wei et al. 2001; Vanstreels et al. 2005; Suslov and Verbelen 2006; Suslov et al. 2009; Kim et al. 2015). The goal of these studies has generally been to infer the microscopic properties of the cell wall from tissue level tensile testing. The results of these studies suggest that the cell wall of onion epidermal cells is anisotropic, with the mean cellulose orientation being along the major axis of the cells (Suslov and Verbelen 2006). This was inferred from the difference in resistance of the tissue against deformation along the two major tissue axes, and supported by observations made with polarized light microscopy (Suslov and Verbelen 2006; Suslov et al. 2009). The fact that tensile testing data at the tissue level have been used to infer the composition of the cell wall underlines the importance of methods for accurate characterization and a better understanding of the tensile behavior of primary plant tissues in general. The epidermis in particular has been shown to control the growth of inner tissue layers (Savaldi-Goldstein et al. 2007). Developing models that can capture the mechanical behavior of the epidermal tissue is therefore essential. Typically, in studies designed to measure the stiffness of the onion epidermis or primary plant tissue in general, the tissue has been considered as linear elastic and the value of Young's modulus is calculated from the slope of the engineering stress–strain graphs. This is

done despite the fact that Young's modulus is only relevant for linear reversible deformations at very small strains. At larger strains, specifically with plastic deformations, the tangent modulus should be used instead. The tangent modulus is defined by the slope of the line tangent to the stress–strain graph at a given point (Gooch 2010). It can be used to evaluate hardening or softening in the plastic domain. When the point of tangency is within the linear elastic range, the tangent modulus becomes equivalent to Young's modulus. However, that requires the deformation behavior of the tissue to be linear, at least within a strain range, which is not always the case for biological tissues, especially at the large elastic strains that they undergo under small stresses.

In this study, we performed uniaxial tensile tests on turgid and plasmolyzed samples prepared from adaxial onion epidermal peels as a model system for isolated primary plant tissue. We first performed the common monotonic tension to failure tensile test to assess parameters such as the elastic modulus, tensile strength, and strain at failure of tissue samples in directions along and transverse to the major axis of cell growth. Further, we performed a series of loading–unloading uniaxial tests, where loading with up to 20% strain was followed by unloading. These cyclic tests were carried out on plasmolyzed samples with the goal to distinguish reversible and irreversible strains from the unloading data. The test data sets were used to calibrate hyperelastic material models, and evaluate their ability to reproduce the observed nonlinear stress–strain behavior of the onion epidermis. The calibration results for the models were confirmed through finite element models of the uniaxial tensile testing.

Materials and methods

Plant material

Fresh onions (*Allium cepa* L.) were obtained from a local supermarket. For consistency, all of the experiments were conducted with adaxial epidermal peels extracted from the equatorial region of the bulbs from scales 2, 3, and 4, counting in from the most external layer.

Sample preparation

A custom cutter was used to consistently cut the onion epidermis samples for tensile tests. The cutter consists of two razor blades that are symmetrically spaced in the center by a glass slide and are curved at the two ends. With this cutter, onion samples were prepared in tapered shapes with widened ends (Fig. 1A). This was to ensure that the strain was mostly concentrated in the gauge length, but importantly, to improve the gripping at the ends and avoid slippage, which is a common issue encountered in tensile testing. Slippage can dramatically alter the tensile testing results, including the slope of the stress–strain graph. Schematics of the sample shape are presented in Figs. 1A and 4A. It should be noted that the sample shape is modified from the common dumbbell shapes used in standardized tensile tests because of challenges with handling the delicate samples. This modification includes the fact that in standard dumbbell shapes, a part of the sample between the gripping ends is considered as the gauge length. In our case, we considered the whole part between the two clamped ends as the gauge length in calculations. The sample was mounted on the device and clamped such that a consistent clamped length of 12 mm was maintained, as observed under the microscope. Clamping was achieved using spring clamps (Fig. 1C), and patches of sandpaper were affixed on the clamps to achieve better and more uniform contact with the sample. We did not use glue to secure the specimens because it was incompatible with the sample moisture and it has the potential to infiltrate and alter the property of the tissue upon curing. Before experiments, the device was calibrated to exclude the weight of the extension, and specifically the clamps, from force measurements. The longitudinal and transverse samples were excised from the region near the equator of the onion scales along and transverse to the bulb axis, respectively (Fig. 1B). The width and length of the gauge area of the specimens were of 0.65 and 12 mm, respectively. The thickness of the epidermis, 0.08 mm, was determined by averaging measurements from micrographs of epidermal cross-section area as well as by using a digital caliper independently for $n = 20$ samples. The number of samples for the monotonic tension to failure tests was $n = 51$ from three different onions. In cases where plasmolyzed and nonplasmolyzed samples were compared, the plasmolysis was carried out by placing the samples in 0.8 mol·L^{-1} mannitol for at least 15 min prior to the experiment. The nonplasmolyzed samples were submerged in dH_2O for the same period. During the experiments, the samples were continuously covered with a layer of liquid using the corresponding solution (mannitol for plasmolyzed or dH_2O for turgid samples) to avoid dehydration. The cyclic tests were carried out on plasmolyzed samples.

Tensile testing

Preliminary tensile tests were carried out on a Liveco Vitrodyne V-200, which is a commercialized miniaturized tensile testing setup developed by Lynch and Lintilhac (1997), that was generously provided by Philip M. Lintilhac, University of Vermont. Further tests were carried out on a tensile testing setup developed in-house. The custom-built tensile device allows us to measure a wide range of forces by its flexible design and interchangeable force sensors. The axial displacement that separates the grips and stretches the sample is generated by a linear motorized stage. Displacement parameters such as velocity and range of displacement are given as inputs to the stage via computer. The stage allows for submicron displacement resolution. The displacement is measured by a linear variable differential transformer (LVDT). The force is measured by a load cell attached to

one of the gripping ends. The load cell is calibrated against a series of known weights prior to the experiment. The force–displacement data of sample stretching are collected at the computer.

For both monotonic and cyclic tests, the speed of loading or unloading of the samples was 20 $\mu m \cdot s^{-1}$. In cyclic tests, the cycle displacement magnitude was 2.5 mm (20% of the gauge length). Real-time observation of tensile tests was carried out using a Zeiss Discovery V8 stereomicroscope. This allowed to detect and exclude from the analysis samples displaying undesirable effects such as slippage, premature failure or rupture near clamps. Observation under the stereomicroscope allowed us to detect any displacement of landmarks that might indicate slippage. Small sawtooth oscillations observed in force–displacement data (e.g., Fig. 2) are, therefore, likely caused by systemic noise. We corroborated this by mounting a loop of elastic rubber on the device (hence no clamping required). Upon opening the jaw, we observed a similar oscillation pattern. The noise in the graph could be alleviated through averaging of the input signal from the force sensor, but we deemed this effect to be inconsequential in this study and prefer to show the original data.

Before applying the load, drops of the appropriate liquid (dH_2O for turgid or mannitol solution for plasmolyzed samples) were added gently on the sample to keep it hydrated. This was repeated during the experiment to keep the sample surface moist. Stress and strain calculated from force–displacement data from tensile tests were used to determine the material parameters of the models as described in the following sections. Raw data of tensile tests are available upon request.

Calculations and in-silico studies

Calculation of stress and strain

The force–displacement data are used to calculate the engineering stress–strain graphs as:

$$\sigma = \frac{F}{A_0} \text{ and } \varepsilon = \frac{\Delta L}{L_0}$$

where σ and ε are the engineering stress and strain; A_0 and L_0 are original cross-section area and gauge length of the specimen; F is force; and $\Delta L = L - L_0$ is the displacement read by the LVDT. The prefix "engineering" as opposed to "true" before stress and strain refers to use of original dimensions (before the sample deformation) in the former as opposed to the use of the instantaneous length and cross-section in the calculation of the latter.

In Fig. 3, first, a 5th order polynomial function was fitted to each individual data set ensuring optimal fit (R^2 value close to 1). The polynomial function parameters were identified, and the function was then used to generate stress data points at regular strain intervals of 0.005 that could then be used for averaging as well as determining the standard deviation.

Hyperelastic curve fitting

The primary plant tissue material was considered isotropic and nearly incompressible. Six hyperelastic formulations were evaluated, in addition to the linear elastic behavior, to simulate the deformation behavior of the adaxial onion tissue: Ogden (orders 1–3), Yeoh, Arruda–Boyce and Neo-Hookean hyperelastic models (Table 1). The Mooney–Rivlin hyperelastic model was also initially considered, but it could not fit the experimental data or was unstable, and hence was not further considered in this study. Hyperelastic material models are widely used to describe the mechanical behavior of soft biological tissues and rubbers (Gasser et al. 2005; Chagnon et al. 2015; Mihai et al. 2017) and are defined by various strain energy potentials, $U(\varepsilon)$. The strain energy function is then used to derive the stress and strains. The Ogden hyperelastic model (Ogden 1972, 1986; Ogden et al. 2004) is a phenomenological (mathematically driven) general hyperelastic model with a strain energy potential defined based on principal stretches in the form of:

$$U = \sum_{i=1}^{N} \frac{2\mu_i}{\alpha_i^2}\left(\bar{\lambda}_1^{\alpha_i} + \bar{\lambda}_2^{\alpha_i} + \bar{\lambda}_3^{\alpha_i} - 3\right) + \sum_{i=1}^{N} \frac{1}{D_i}(J_{el} - 1)^{2i}$$

where $\bar{\lambda}_i$ represent the deviatoric principal stretches; $\bar{\lambda}_i = J^{-\frac{1}{3}}\lambda_i$, λ_i are the principal stretches; J is the total volume ratio; and J_{el} is elastic volume ratio; N is a material parameter; and μ_i, α_i, and D_i are temperature-dependent material parameters (Abaqus theory manual 2019). For a physically realistic response and material stability, for $N \leq 2$ (Ogden et al. 2004):

$$\mu_i \alpha_i > 0$$

For instance, for the first-order Ogden model, we used the constraint $\mu_1\alpha_1 > 0$. By assuming an incompressible material behavior, D_i, were excluded from the optimization process and the material parameters optimized in the curve fitting for this model were μ_i and α_i. For numerical purposes, a negligible compressibility was assigned to D_1 in all models when applicable ($1e^{-2}$ Pa^{-1}). Therefore, the number of parameters for the first, second, and third order Ogden model are 2, 4, and 6, respectively. It should be noted that, while the Ogden model is generally very capable in fitting a wide range of experimental data, it should be used with caution. Specifically, to calibrate this model, generally, a combination of two or more different types of experiments such as combinations of uniaxial, biaxial, or planar tension or other tests are required. The parameters obtained from calibration of this model based only on one type of experiment, such as uniaxial tension as is the case in this study, can generate considerable errors in predicting stresses for the other types of deformations. Therefore, this model is

generally used when data from several types of mechanical tests are available (Dorfmann and Muhr 1999; Bergström 2015; Shahzad et al. 2015).

The Yeoh hyperelastic model (Yeoh 1993) is an invariant-based strain energy potential expressed as:

$$U = \sum_{i=1}^{3} C_{i0}(\bar{I}_1 - 3)^i + \sum_{i=1}^{3} \frac{1}{D_i}(J_{el} - 1)^{2i}$$

where C_{i0} and D_i are temperature-dependent material parameters, and $\bar{I}_1$ is the first deviatoric strain invariant defined as:

$$\bar{I}_1 = \bar{\lambda}_1^2 + \bar{\lambda}_2^2 + \bar{\lambda}_3^2$$

Considering incompressibility for this model, three parameters of C_{i0} are to be identified by fitting to the experimental data. As can be seen from the formulation, this model does not rely on the second strain invariant. Hyperelastic models that are independent of the second invariant are generally suggested to be suitable when only one type of experiment is available for calibration (Bergström 2015). As in this study only uniaxial test data were produced, and due to a relatively good fit of this model to our experimental data (see Results), we chose this material model for identification of the onion epidermis hyperelastic constants.

The Neo-Hookean model is a simple hyperelastic model that is, like the Yeoh model, a special case of reduced polynomial strain energy potential, defined as:

$$U = C_{10}(\bar{I}_1 - 3) + \frac{1}{D_1}(J_{el} - 1)^2$$

Because of its simplicity, the Neo-Hookean material model is generally used when accurate material data and experiments are lacking. When D_1 is removed from the calibration process by considering a slight compressibility, the only material parameter to be identified for this model is C_{10}. This is similar to the linear elastic case defined by Young's modulus E, when the Poisson's ratio (ν) is assigned a value close to 0.5.

Lastly, the Arruda–Boyce or eight-chain (Arruda and Boyce 1993) hyperelastic strain energy potential is defined as:

$$U = \mu \sum_{i=1}^{5} \frac{C_i}{\lambda_m^{2i-2}}(\bar{I}_1^i - 3^i) + \frac{1}{D}\left(\frac{J_{el}^2 - 1}{2} - \ln J_{el}\right)$$

where C_i are constants as follows:

$$C_1 = \frac{1}{2}, C_2 = \frac{1}{20}, C_3 = \frac{11}{1050}, C_4 = \frac{19}{7000}, C_5 = \frac{519}{673750}$$

This is a micromechanically (in contrast to phenomenologically) motivated model because it takes into account the molecular network of the material. Eliminating D from the unknowns, as in the previous models, leaves two material parameters to be determined: μ and λ_m, the shear modulus, and the network locking stretch parameter, respectively. We assigned a constant value of 1 to λ_m.

MCalibration 5.1.2 software (Veryst Engineering, Needham, Massachusetts, USA) was used to fit linear elastic and hyperelastic material models to stress–strain data obtained from cyclic tensile testing. Drucker's stability of the hyperelastic models with the identified material parameters was confirmed for uniaxial tension up to 50% strain, exceeding the strains relevant in our experiments (20% strain, a fraction of which was deemed elastic, Fig. 2). The function to be minimized in MCalibration was set as the mean square difference (MSD) between the experimental data and the output of the hyperelastic function being calibrated. MCalibration was set to use an extensive search for optimal parameters minimizing the fitness function, including an initial random search followed by Levenberg–Marquardt and Nelder–Mead simplex methods.

In cyclic tensile tests, loading was performed up to 20% strain for both transverse and longitudinal samples (Fig. 2), followed by unloading. To limit the fit of the hyperelastic models to the reversible or elastic parts of deformations, we attempted to separate the elastic and plastic strains. To this end, we used the recovered strain (ε_{EU}, Fig. 2) from the unloading part as an indicator of the elastic range of deformations in both loading and unloading. In addition to this, for the loading part of the data, we examined and excluded strains at which the slope of the stress–strain curves changed. This change, usually towards a lower slope marking a softening at the end of the cycle, is indicative of damage. It should be noted that, because of such effects, the recoverable strain from unloading can be different from the true elastic range of loading before permanent changes in the material have occurred. However, at this stage and for the purpose of this paper, we considered this simplification reasonable. In future studies, it may be beneficial to use viscoplastic models that take into account the material damage, but this approach was beyond the scope of this study.

We wanted to include ranges in which all samples were within the elastic limit so that we could fit the hyperelastic models to all data sets simultaneously. After determining the elastic range based on the above approach, we limited the fitting of the hyperelastic models to ranges of 8% and 12% strains for longitudinal and transverse specimens, respectively. The lower value considered for the longitudinal samples was necessary because they underwent plastic deformation and failure at smaller strains compared with the transverse samples

(Fig. 1H). The material parameters found at this step were used as initial inputs for finite element models of uniaxial tensile tests in Abaqus (Dassault Systèmes, Simulia Corporation, Providence, Rhode Island, USA, 2019) to evaluate the results obtained from curve fitting (Fig. 4) when realistic sample geometry and boundary conditions are considered. After this confirmation, the Ogden ($N = 1$) and Yeoh models were fitted for each case of transverse and longitudinal, loading and unloading, simultaneously to all experimental data, using MCalibration (Fig. 5; Tables 2 and 3).

Finite element analysis

The Abaqus finite element package was used for all modeling steps from defining geometry to post-processing (Fig. 4). Abaqus/Standard solver was used for quasi-static finite element simulations. The tissue geometry and dimensions were as described in the sample preparation section (Fig. 4A). Ignoring cellularity, the tissue was considered as a homogeneous isotropic continuum material. C3D20RH, 3D continuum finite elements were used to discretize the geometry. The hyperelastic model parameters were estimated from the initial curve fitting as described in the previous section and input in Abaqus. Simulations were run on a Windows 10 workstation with dual Xeon E5-2643 v4 processors and 128 GB of 2400 MHz DDR4 physical memory.

Results

The epidermal tissue is mechanically anisotropic but the mechanical link between tissue- and cell-level anisotropy is obscure

The difference in mechanical properties of onion epidermal tissue along and transverse to the main axis of cell elongation has been linked with the net cellulose orientation in walls of individual cells comprising the tissue (Suslov and Verbelen 2006; Suslov et al. 2009). To assess the mechanical properties of the onion epidermal tissue, we first performed strain-to-failure monotonic tensile tests. Tapered samples (Fig. 1A) from the adaxial onion epidermis along and transverse to the major cell growth axis (Fig. 1B) were mounted on the tensile device and stretched to rupture (Figs. 1C–1E). Force–displacement data from tensile tests were recorded and used to obtain the stress–strain graphs (see Materials and methods and Fig. 1F).

To calculate Young's modulus as a means to compare the stiffness of the samples along the two distinct directions, similar to previous studies, we had to find the slope of the linear portion of the stress–strain curves. However, in most cases, no perfectly linear portion could be found because the stress–strain data were nonlinear. Therefore, we chose segments of the graphs that seemed close to linear below 25% strain, typically between 10%–15% strains. The results for the tangent modulus of the onion epidermis measured in this way, indicated that the stiffness of the onion epidermis in the transverse direction appeared to be 44% lower than that of the longitudinal direction ($p < 0.005$) (Fig. 1G), which is qualitatively in agreement with previous findings (Vanstreels et al. 2005). Upon plasmolyzing the samples, however, the difference between the transverse and longitudinal tangent values decreased to 24%, and the difference was statistically insignificant ($p > 0.05$). The transverse samples showed higher strains at rupture compared with the longitudinal samples in both plasmolyzed and turgid cases (Fig. 1H). The difference was statistically significant ($p < 0.05$) for the turgid, but not for plasmolyzed samples ($p > 0.05$). Importantly, the maximum stress reached before rupture in these experiments was higher for transverse samples in both turgid and plasmolyzed tissues (Fig. 1I). This result is interesting considering the initial higher stiffness of the tissue and the reported mean orientation of cellulose alignment in the longitudinal direction (Suslov and Verbelen 2006; Suslov et al. 2009). However, the difference between the ultimate stress of the transverse and longitudinal groups for both cases of turgid and plasmolyzed tissues was statistically insignificant ($p > 0.05$).

Force–deformation behavior of onion epidermal tissue is nonlinear

From the experiments described in the previous section, we retained that determining a linear elastic strain range for the onion tissue was challenging in many cases. The reason was the lack of a substantial or detectable linear range in the stress–strain graphs of these samples. Further, from the monotonic tension-to-failure tests, the reversible range of the deformations cannot be determined to ensure that the deformations at which the elastic parameter is calculated are truly reversible. For this reason, we performed a cycle of loading–unloading on plasmolyzed samples. The loading cycle was limited to 20% strains to avoid rupturing the sample. The results, in general, demonstrated nonlinear loading–unloading paths and residual (plastic) deformation upon unloading for both the transverse and longitudinal samples (Fig. 2). As will be discussed later, and can be seen from Fig. 2, the unloading part of the data differs significantly from the loading part. This is in part due to hysteresis effects, even if deformations are limited to the elastic range. It was observed that at the strains we had considered to measure the tangent modulus in monotonic tests, in many samples the plastic deformation may have already initiated. Indeed, the result of cyclic loading–unloading shows that samples exhibit average (SD) reversible strains of 11.5% (±1%) and 15% (±1%) for the longitudinal and transverse specimens, respectively, as determined from the unloading paths (Fig. 2). Therefore, from this point onward, we limited the strains for (nonlinear) elastic parameter identification within these ranges. Specifically, we limited the estimation of parameters to a subset of these strains, namely to 8% and 12% for the longitudinal and transverse samples, respectively, to

Fig. 1. Uniaxial tensile testing on adaxial onion epidermis. (A) Uniaxial tensile specimens cut with tapered ends using a custom cutter. The dimensions of the gauge region used for the calculation of stress and strain are shown. (B) Transverse and longitudinal onion epidermis tensile samples were taken from the equator region of the onion scales, along and perpendicular to the axis of the bulb, respectively. (C) The custom-built device allows for tensile loading of small plant samples while observing the process under a stereomicroscope. The white rectangle indicates the mounted sample. (D) Longitudinal onion epidermis sample mounted between the two gripping ends of the tensile device. (E) Closeup of a turgid longitudinal (E1) and a plasmolyzed transverse (E2) onion sample mounted on the device. Scale bar = 200 μm for E1 and E2. (F) Example of stress–strain graphs of turgid adaxial onion epidermis for transverse and longitudinal samples. (G) The tangent modulus was calculated for onion samples from a linear portion of the engineering stress–strain curves. The stiffness was higher along the longitudinal cell axis compared with the transverse orientation. In the plasmolyzed tissue samples the difference was smaller. (H) Average rupture strains of plasmolyzed and nonplasmolyzed samples. Transverse samples tolerated higher strains prior to rupture. (I) Transverse specimens tended to rupture at slightly higher stresses compared with longitudinal specimens in both the turgid and plasmolyzed groups. Bars show the standard error; n = 51 samples (10, 12, 17, and 12 samples for the transverse, plasmolyzed transverse, longitudinal, and plasmolyzed longitudinal samples, respectively). [Colour online.]

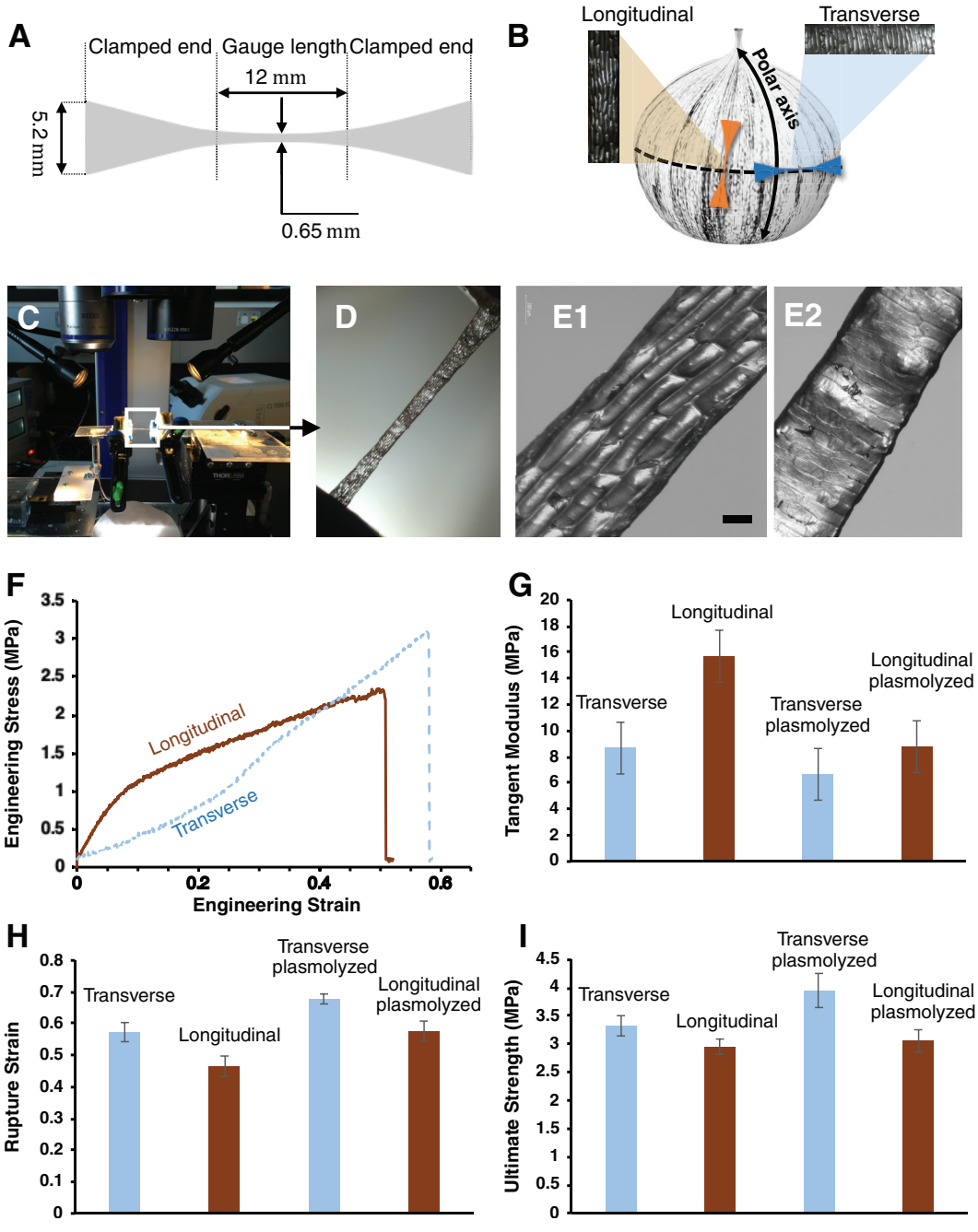

Fig. 2. Typical stress–strain graph resulting from a single cycle of loading–unloading on a longitudinal specimen of plasmolyzed adaxial onion epidermis. The curve starts with a nonlinear portion exhibiting strain stiffening, followed by a change in slope demonstrating softening (horizontal dotted line). The unloading curve takes a different path showing substantial hysteresis and residual (plastic) deformation. The vertical dotted lines mark elastic strain recovered upon unloading (ε_{EU}) used to determine the elastic strain range for both loading and unloading parts. It should be noted, however, that material undergoes changes upon loading, and this elastic strain might not be fully relevant to the elastic strains in loading.

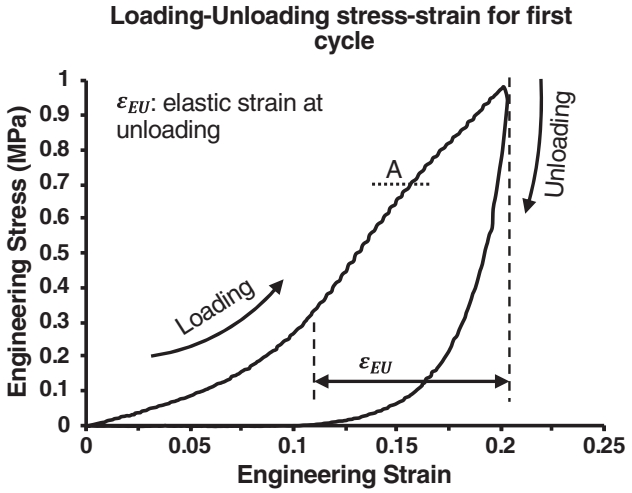

ensure that the deformations in all of the samples were within the reversible range (see Materials and methods).

Separating the reversible and irreversible portions of deformation from loading–unloading data, we observed that the elastic deformation of tissue for both transverse and longitudinal samples is highly nonlinear, and therefore cannot be described sufficiently with a single linear elastic modulus (Fig. 3). Nonlinear stress–strain behavior is known to be inherent to many biological materials, including soft tissues (Fung 1967). Hyperelastic material models comprise a large class of elastic material models that are commonly used to describe the deformation behavior of elastomers and biological tissues that undergo large and nonlinear deformations under relatively small stresses (Bergström 2015; Mihai et al. 2017). To assess the performance of the hyperelastic models with respect to reproducing the deformation of onion epidermis, we fitted several hyperelastic formulations as well as the linear elastic model to the unloading part of the uniaxial test of a transverse specimen. We chose the unloading path at this stage to ensure that deformations were elastic, but eventually applied the calibration to the loading paths as well. The parameters for each material model were determined first using MCalibration through an optimization process (see Materials and methods and Table 1). To further evaluate the output of the material models with the identified parameters, a 3D finite element model of the uniaxial test specimen was developed in the finite element package Abaqus, and the model was run with the tested material models. Figure 4 depicts the force–displacement output of different material behaviors plotted against the experimental data. Specifically, the Yeoh model with three variables, and the three Ogden models with two, four, and six variables (see Materials and methods) all appeared to capture the trend of the experimental data points (Table 1). The linear elastic model, as well as the Neo-Hookean and Arruda–Boyce hyperelastic models, on the other hand, did not reproduce the trend observed in the experimental data, and specifically the upturn or strain stiffening, for any input parameter.

Yeoh and Ogden hyperelastic models can reproduce the elastic uniaxial test data

A number of criteria are often cited for the proper choice of hyperelastic models (Shahzad et al. 2015). The most important ones in our context are the ability of the model to provide a "complete" description of the material deformation behavior. The term "complete" encompasses two aspects of the model properties: being able to capture the entire range of stress–strain data at small, intermediate, and large strains, but importantly also to produce reliable predictions for other modes of deformations with inputs based on model calibration to only one or a limited number of experiment types. The latter entails, for instance, the ability of a model to predict the biaxial stress–strain behavior of the material reasonably well, based on the data from calibration to uniaxial tensile test data only. Finally, a smaller number of parameters in each model is desirable to reduce the number of experiments needed for model calibration.

The results in the previous section indicate that Ogden and Yeoh hyperelastic models could reproduce the observed force–deformation behavior of the adaxial onion epidermis under uniaxial tension. The true value of a model, however, lies in its ability to explain observations and (or) predict outcomes with a minimum number of required parameters (Howard 2014). It is particularly so in the absence of sufficiently diverse types of experimental data to disentangle the influence of different parameters and to evaluate their potential in predicting other modes of deformation. As described in Materials and methods, the use of the Ogden model is generally preferred only when data from at least two types of tests are available, such as from uniaxial and biaxial tension. For this reason, and as the added number of parameters is not justified, we only considered the first order of the Ogden model ($N = 1$) further in this study to fit the loading and unloading data of the uniaxial tension test on onion epidermis. Excluding the parameter controlling the compressibility, D_1, the first order Ogden model can be defined using two parameters, μ_1 and α_1 (refer to Materials and methods). The Yeoh hyperelastic model also

Fig. 3. Stress–strain data for single-cycle loading and unloading uniaxial tests for transverse (A and B) and longitudinal samples (C and D). The strain on the transverse specimens was applied at 12%, and on the longitudinal at 8%, because the former tolerates larger strains before undergoing permanent deformation. The stress–strain data show varying degrees of nonlinearity for the loading–unloading paths of the transverse and longitudinal samples. The bars indicate the standard deviation and show that variations in force measurement in samples increase at larger strains; n = 30 (14 longitudinal and 16 transverse specimens).

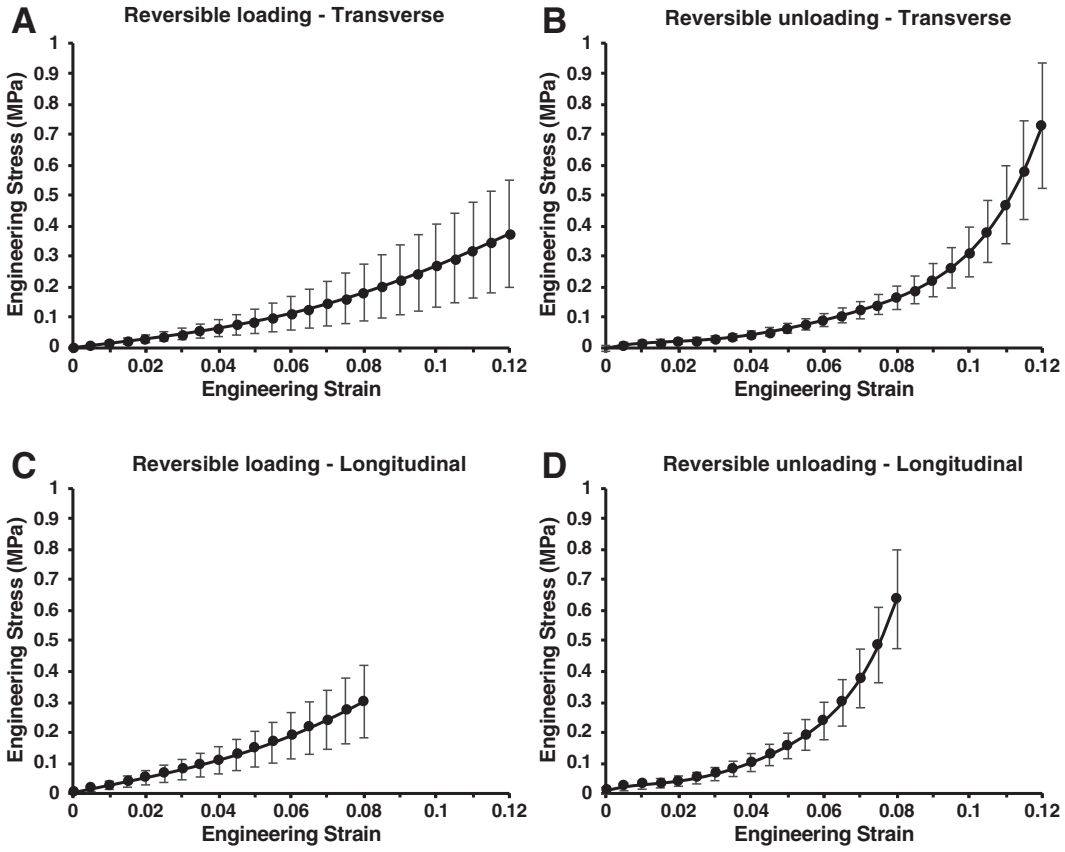

Table 1. A set of optimal parameters from fitting the various hyperelastic and linear elastic models to an example unloading stress-strain data set of a transverse epidermis tensile specimen.

Models	Parameters								
Ogden (N = 1)	μ_1 = 0.24	α_1 = 39.7	$D_1 = 1e^{-2}$						
Ogden (N = 2)	μ_1 = 0.214	μ_2 = 0.03	α_1 = 41.08	α_2 = 0.474	$D_1 = 1e^{-2}$	D_2 = 0			
Ogden (N = 3)	μ_1 = –0.0	μ_2 = 0.05	μ_3 = 0.36	α_1 = –59.6	α_2 = 55.1	α_3 = 14.71	$D_1 = 1e^{-2}$	D_2 = 0	D_3 = 0
Yeoh	C_{10} = 0.26	C_{20} = –1.0	C_{30} = 271	$D_1 = 1e^{-2}$	D_2 = 0	D_3 = 0			
Arruda-Boyce	μ = 0.59	λ_m = 1	$D = 1e^{-2}$						
Neo-Hookean	C_{10} = 0.99	$D_1 = 1e^{-2}$							
Linear Elastic	E = 6.23	ν = 0.49							

Note: All of the models are considered as nearly incompressible. As a result, D values and the Poisson's ratio, ν, were excluded from optimization in curve fitting. The network stretch parameter, λ_m, of the Arruda–Boyce model was also assigned a default value of 1 and was excluded from curve fitting optimization. Values for μ_i, C_{ij} and E are in MPa; values for D_i are in MPa^{-1}.

seemed to produce results similar to the Ogden (N = 1) model (Fig. 4B). Unlike the Ogden model, however, the Yeoh model, an invariant-based hyperelastic formulation independent of the second strain invariant, is deemed reliable even with only one type of test data available for calibration (Bergström 2015). Therefore, the Yeoh model was also considered for material parameter identification (Table 3). To obtain average model parameters, each model was fitted to all data series simultaneously for each case of loading and unloading portions of the tensile tests for transverse and longitudinal samples (Fig. 5).

The values of parameters identified for the Ogden (N = 1) model are presented in Table 2, along with parameters for this model for soft tissues from other studies for comparison. A considerable variation can be observed between the model parameters for different tissues. Nevertheless, the values of μ_1 and α_1 for the adaxial onion epidermis samples are well within the range of values identified for other materials. To evaluate the

Fig. 4. (A) Geometrical representation of the specimen used for finite element analysis. (B) Force–displacement data predicted by the finite element model for various linear and nonlinear material models with inputs from curve fitting compared with the experimental data of the unloading portion of a transverse onion sample (red data points). The values from curve fitting are presented in Table 1. [Colour online.]

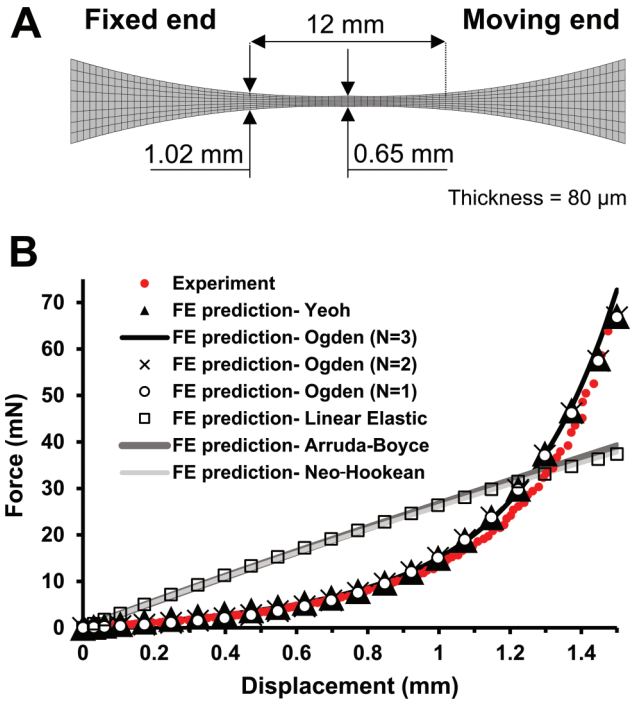

influence of each of the parameters of the Ogden model on the stress–strain outcome, a parametric study was performed by varying each parameter by 50% about the average value found from a group of samples, keeping the other parameters constant. It can be seen that, while increasing the parameter μ_1 (related to the shear modulus) increases the stiffness and therefore the stress of the model, α_1 controls the strain-stiffening and nonlinearity of the response, with force–displacement behavior approaching a linear behavior with α_1 values approaching zero (Fig. 6). The parameter μ_1 was found to be larger for longitudinal specimens (0.724 MPa) compared with the transverse samples (0.554 MPa). For both groups, the loading path was defined with a higher μ_1, and the unloading path with a higher nonlinearity parameter α_1. Interestingly, while the loading path is more linear for longitudinal samples, a considerable nonlinearity is demonstrated by the unloading path of force–displacement data of this group.

Discussion

Modeling and experimental studies are required to investigate the origins of plant tissue mechanical anisotropy

In this study, we adopted a phenomenological approach to investigate the nonlinear tensile behavior of the onion epidermis. Like all plant tissues, the onion epidermis is not a homogeneous continuum, as assumed by the constitutive material models used in this study. The microstructural features of the cellular tissue are certain to influence the deformation behavior of the tissue under load. These features are of both material and geometrical nature and are relevant at multiple scales. The tissue is cellular thus featuring load-bearing structures (apoplast) and liquid-filled cavities (symplast) and the cell wall proper is heterogeneous and has the potential to be anisotropic. Combined, these features cause non-uniform distribution of stress and strain fields at subcellular scale. However, in this study our aim was to investigate how the tissue deforms globally under load rather than the microstructural underpinnings of its behavior. Therefore, we considered the tensile behavior of the tissue as a whole using continuum models, disregarding any phenomena at the microscopic scale, such as cell wall anisotropy or cell shape. We evaluate several material models with regards to their ability to describe the recoverable strains under uniaxial tension. This has fundamental significance because determining the appropriate constitutive behaviors is an essential part of modeling and interpreting deformation of plant cells and tissues (Bidhendi and Geitmann 2018*a*).

We evaluated the extent to which the epidermis tissue can be regarded as a linear elastic material. The tangent modulus calculated from the monotonic tension-to-failure tests demonstrated a considerable anisotropy between the longitudinal and transverse samples (Fig. 1G). However, the difference was significantly diminished upon plasmolysis. It is intuitive for the loss of turgidity to reduce the apparent stiffness of the tissue. However, the mechanics underlying the observed disproportionate stiffening of tissue in two directions by turgidity requires further investigation. It is plausible for the effect of turgor to either mask or amplify subtle differences by putting the cell wall under pre-stress. It should be noted, however, that as mentioned previously, measurement of the tangent modulus from the experimental data was challenging due to the absence of a true linear behavior in many cases, and was dependent on the judgment of the experimenter to locate an approximately linear region. As a result, the reduced difference between the longitudinal and transverse stiffness upon plasmolysis may be due to measurement errors, especially given that the plasmolyzed samples exhibited a higher nonlinearity. The nonlinear Ogden model parameter μ_1 showed an increase in the longitudinal direction for the loading path. This further confirms that a stiffness anisotropy between the samples exists, without needing to resort to a linear elastic modulus. However, further studies are required to evaluate turgid samples and to investigate whether the turgor increases the directional stiffness of the tissue disproportionally.

Fig. 5. First-order Ogden hyperelastic ($N = 1$) and Yeoh ($N = 3$) models were fit to all (A) transverse loading (B) transverse unloading, (C) longitudinal loading, and (D) longitudinal unloading data series. The material parameters were identified inversely by minimizing the mean square difference (MSD) function between the experimental data points and the outcome of the hyperelastic material functions. The material parameters for this model are provided in Tables 2 and 3; $n = 30$ (14 longitudinal and 16 transverse specimens). [Colour online.]

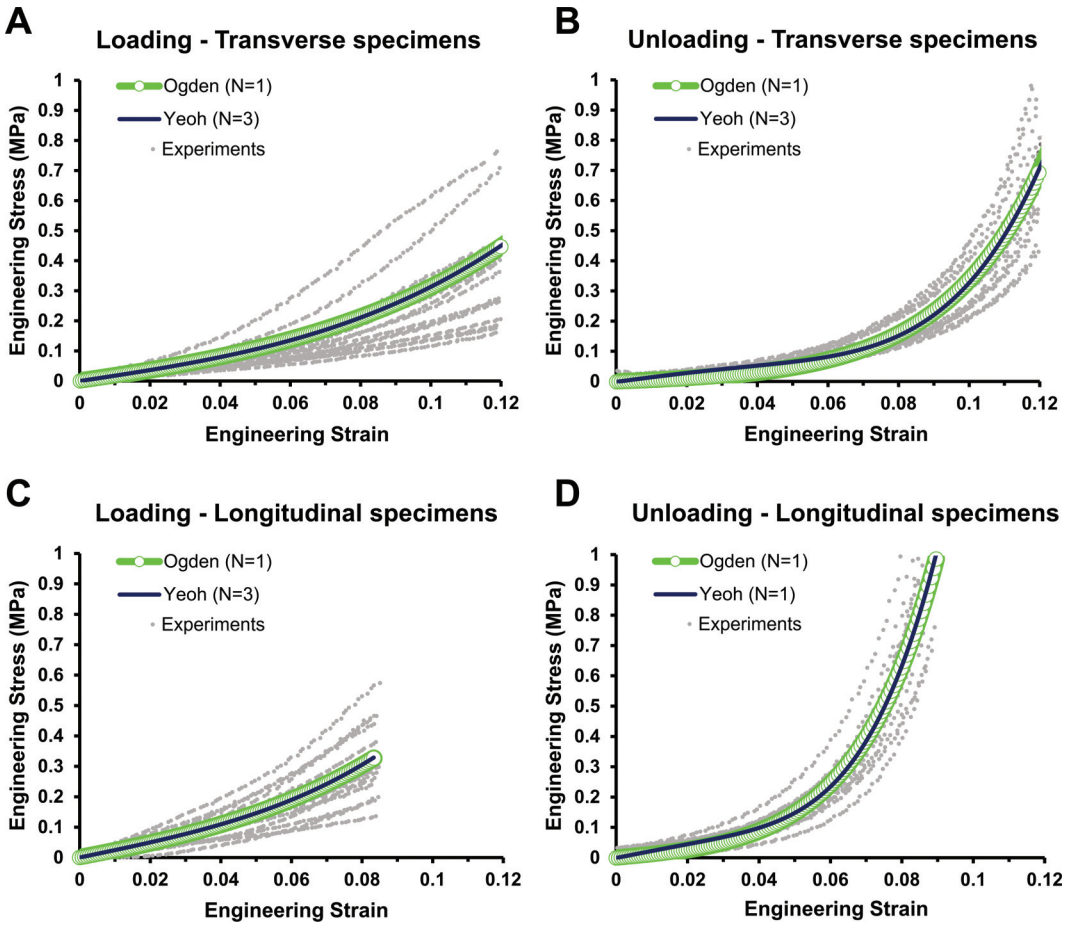

Table 2. Optimal parameters found for the first order Ogden model ($N = 1$) for plasmolyzed adaxial onion epidermal specimens cut along (longitudinal) or perpendicular to the axis of the onion and selected other biological tissues.

	Ogden model ($N = 1$)		
Parameters	μ_1 (MPa)	α_1	D_1 (MPa^{-1})
Transverse onion epidermis (loading; this study)	0.554	16.1	$1e^{-2}$
Transverse onion epidermis (unloading; this study)	0.145	41.92	$1e^{-2}$
Longitudinal onion epidermis (loading; this study)	0.724	21.85	$1e^{-2}$
Longitudinal onion epidermis (unloading; this study)	0.33	52.22	$1e^{-2}$
Human foot tendon (Morales-Orcajo et al. 2017)	33.16	24.89	$12e^{-5}$
Porcine skin (Remache et al. 2018)	0.69	23.2	0
Human epidermis (Groves et al. 2012)	4.099	2.98	0
Human dermis (Groves et al. 2012)	0.022	3.28	0
Porcine cortex (Coats and Margulies 2006)	$167e^{-6}$	0.013	0

Note: Values for D_1 were not included in the optimization process for onion epidermis, and the material was considered nearly incompressible.

The stiffness anisotropy observed between the longitudinal and transverse tissue specimens is thought to be related to the cell wall anisotropy and, specifically, to a net longitudinal orientation of cellulose microfibrils (Suslov and Verbelen 2006; Suslov et al. 2009). However, comparing the ultimate strength from monotonic tensile tests of the samples did not confirm this. Particularly, if the net orientation of cellulose was in the longitudinal direction, the samples excised in this direction were expected to exhibit a considerably higher ten-

Table 3. Optimal parameters found for the Yeoh model ($N = 3$) for plasmolyzed adaxial onion epidermal specimens cut along the longitudinal axis or perpendicular to the axis of the onion and for porcine skin for comparison.

	Yeoh model ($N = 3$)		
Parameters	C_{10}	C_{20}	C_{30}
Transverse onion epidermis (loading; this study)	0.29	3.27	$2e^{-4}$
Transverse onion epidermis (unloading; this study)	0.26	–4.73	257
Longitudinal onion epidermis (loading; this study)	0.406	6.68	34
Longitudinal onion epidermis (unloading; this study)	0.394	–4.44	$1.22e^{3}$
Porcine skin (Remache et al. 2018)	0.26	15.5	1.75

Note: Values for D_1–D_3 are not included in the optimization process for onion epidermis. $D_1 = 1e^{-2}$ MPa^{-1}, and the other values were zero. Values for C_{10}, C_{20}, and C_{30} are in MPa.

Fig. 6. Parametric studies investigating the influence of the material parameters in the first-order Ogden ($N = 1$) model. Each of the model parameters, (A) α_1 and (B) μ_1 were varied by 50% around the average value found from optimization while keeping the other parameter constant. Both parameters significantly affected the model results; α_1 controlled the nonlinearity of the stress–strain curve with the model approaching a linear behavior as values for α_1 approached zero.

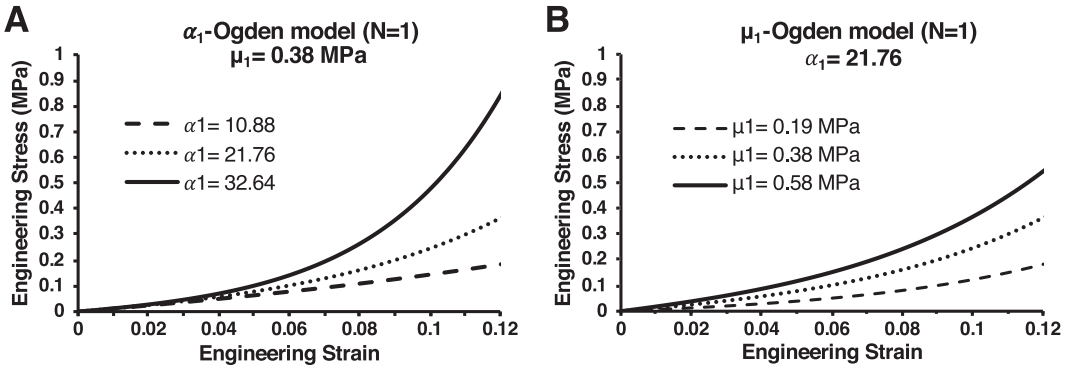

sile strength than those prepared in the perpendicular direction to the mean cellulose orientation. A recent study on thin anisotropic films with cellulose nanofibers showed anisotropic samples to possess strengths that in the direction of fibers were nearly three times those of films with randomly oriented cellulose (Zhu et al. 2017). In our study, the transverse specimens demonstrated a tendency towards a higher tensile strength (determined by maximum stress reached before rupture) than the stiffer longitudinal specimens, although the difference between these two sample groups was statistically insignificant. Because the cell wall is a complex composite material of various polysaccharides, a direct conclusion is challenging. For instance, the observed lack of a significant difference between the tensile strength of longitudinal and transverse samples may mean that rather than cellulose determining the failure behavior, another wall polymer is the weakest link in both directions and fails first. However, these results may also mean that inferring the cell wall anisotropy and net orientation of cellulose microfibrils from a stiffer behavior of tissue in a given direction may not be a straightforward procedure, and that cell-level details may need to be incorporated into calculations.

Deformation behavior of the isolated epidermis is nonlinear

Biological tissues often demonstrate a nonlinear deformation behavior (Fung 1967). While the concept of nonlinearity of plant material and specifically the primary plant material has been put forward in the past (Spatz et al. 1999; Kierzkowski et al. 2012), to our knowledge, this is the first study to investigate this phenomenon and quantify the nonlinear deformation behavior of the primary tissue in the reversible regime observed in tensile testing. The nonlinear behavior is observed in different studies reporting similar stress–strain curve patterns (Yuan et al. 2001; Ryden et al. 2003; Vanstreels et al. 2005; Abasolo et al. 2009; Saxe et al. 2016). Yet, many more studies do not illustrate the stress–strain curve behavior, and only report Young's modulus values in bar graphs, thus tacitly assuming a linear behavior. In these studies, either a linear region of the curve was identified to find the slope for calculation of Young's modulus, or a region of the curve was chosen that showed a maximum, linear slope (Ryden et al. 2003). While some plant tissues, especially those containing the secondary cell wall, may exhibit a predominantly linear elastic behavior, many primary plant tissues behave nonlinearly. While determining the stiffness value allows for a rough comparison between samples, it may not be suitable for a quantitative approach to predict tissue behavior. In this study, we observed that a region that is deemed linear and considered for slope calculation can belong to strains already beyond the reversible regime. This became evident from the loading–unloading data.

Among the hyperelastic material models tested in the present study, the Ogden and Yeoh models fit the experimental data successfully. For each of the four cases, the models were fitted to all experimental data simultaneously. The alternative, obtaining material coefficients by averaging the model results fitted to individual data sets needs to be avoided because it is likely to give rise to erroneous or nonphysical outcomes (Robertson and Cook 2014). The Yeoh model is independent of the second deformation invariant, and is suggested to be suitable when only one type of experimental data are available for calibration (Bergström 2015). For the Ogden model or hyperelastic models that rely also on the second deformation invariant in the formulation of their strain energy functions, however, data from more types of experiments, such as uniaxial and biaxial tensile data, are required to reliably calibrate the model parameters. The value of these models when calibrated based on limited experimental data are questionable because they can make erroneous predictions for other deformation modes (Dorfmann and Muhr 1999). The parameters identified for the Ogden and Yeoh models for adaxial onion epidermis fall within the range reported for other biological tissues (Tables 2 and 3). Specifically, the parameters for the loading path from the Ogden model are close to porcine skin. The unloading path of tensile tests showed a reduced μ_1 (Table 2). This is in agreement with a reduced "cyclic elastic modulus" compared with the loading slope reported by Vanstreels et al. (2005). Further studies are required to assess whether the Yeoh and Ogden model parameters obtained in this study can reproduce the other deformation modes of the plant epidermal tissue, such as biaxial tension.

Limitations and opportunities for prospective studies

A major simplifying assumption made in this study was to consider the epidermis as a uniform material, ignoring the cellularity of the tissue. Because of this, the thickness of the tissue, including the cell lumens, is considered as the effective load-bearing thickness used in stress calculations. In reality, the effective cross-section is the cumulative thickness of all cell walls in the cross-section, and the liquid-filled lumens do not contribute to the load-bearing. As a result, the effective cross-sectional area bearing the load is considerably smaller than the values used in this study, and the resulting engineering stress values found in this and similar studies reflect the tensile properties of the epidermal tissue rather than the cell wall proper. On a related note, the thickness of the epidermis measured in this study was derived from the turgid samples. This was because with the methods we used to measure the epidermis thickness using digital caliper and stereomicroscope (see Materials and methods), measurement on and handling of plasmolyzed samples was problematic. More importantly, because plasmolysis does not change the effective thickness of the sample, namely the collective thickness of the cell walls, we did not see any reason to change the effective cross-section for the plasmolyzed samples. This, however, independently emphasizes a source of underestimation for the stiffness values identified using onion epidermis in this study. Measuring the proportion of the cell wall to the overall volume of the sample, similar to that carried out by Saxe et al. (2016), is one way to correlate the tensile properties measured at the tissue level to the cell-wall level properties.

Kim et al. (2015) reported an average Young's modulus of 80 MPa for the outer (abaxial) onion epidermis in the longitudinal direction, much higher than our equivalent value of tangent modulus. However, the average thickness of the onion epidermis used in their study was reported to be 7 μm, indicating that during the separation from the scale, only half of the epidermis had been removed. Hence, essentially, only the outer periclinal walls were measured, as was the case for another study by Zhang et al. (2016). Therefore, the stiffness value reported by Kim et al. (2015) may be more closely related to the material properties of the cell wall proper, because the cell lumen is removed from the cross-section consideration, whereas our data, as mentioned, apply to the tissue. While an interesting outcome, this is not the point we pursued in this study, and as mentioned, the deformation behaviors of the onion epidermis are more accurately described using nonlinear material behavior. In that case, a more reliable comparison between different epidermal layers can be performed. For these reasons, in this study, the trends and patterns should be held to a higher significance than the absolute values themselves. Further, the values reported in this study are average properties, because the samples were taken from different onion scales. Whether the onion epidermis behaves differently in different scales needs further investigation.

The shape of the tensile specimen used in this study was modified from the standardized dimensions, such as dumbbell shapes, which are specified in standards such as ASTM D638 (ASTM 2014). The standardized sample dimensions are used to avoid nonhomogeneous stress fields and end effects resulting in calculation errors when deducing parameters from tensile tests. Here, we used a tapered version of the standard dumbbell shape to avoid inducing tear and damage in the fragile material during cutting. As with a true dumbbell shape, the wider ends of our tapered specimens allowed us to considerably improve the gripping and reduce slippage, which is a common challenge in tensile testing. Also, the width of the sample was slightly larger near the clamps. Our finite element model based on realistic sample shape produced results that were close to the MCalibration hyperelastic fitting results for uniform width (Fig. 4). Not

surprisingly, owing to the slightly wider ends in the gauge length, the finite element model of the tapered sample behaves slightly stiffer than one with a uniformly-wide gauge length. Inverse finite element analysis could be used to quantify the difference between the identified values and those based on the detailed geometry. However, as the difference was negligible and was not the goal of the study, we did not pursue this further. Developing methods for standard plant tissue sample preparation and use of standardized sample dimensions are warranted in future studies.

Another point to consider is the limit of the application of the proposed model parameters in this study. While we obtained very good fits between the output of the hyperelastic material models and the experimental data, the parameter identification process was based on only one type of experiment: uniaxial tension test. As discussed, some of the hyperelastic models may be less useful when data from limited test types are available. Further, in living plant cells, the cell wall experiences a biaxial stress state due to the turgor, which justifies the development of methods to incorporate the biaxial stress of the anisotropic cell wall. Lastly, the accuracy of models could be increased by accounting for viscoelastic and plastic effects. While we fitted hyperelastic curves to loading and unloading part of data separately, proper visco-elastoplastic models can simulate the whole cycle, accounting for plastic and hysteresis effects, moving toward a "fuller" picture of the cell wall deformation behavior as a result.

Author contributions

A.J.B. and A.G. designed the study; A.J.B. performed the tensile experiments, curve fitting, and simulations; H.L. performed the cyclic tests; A.J.B. and A.G. wrote the manuscript.

Acknowledgements

This project was supported by a Discovery grant from the Natural Sciences and Engineering Research Council of Canada (NSERC) and by the Canada Research Chair Program. We would like to thank Dr. Philip M. Lintilhac for generously providing us with the Vitrodyne tensile testing device (Lynch and Lintilhac 1997; Wei et al. 2001) for preliminary tests. We would like to acknowledge the support of Dr. M. Shafayet Zamil in setting up the in-house tensile device, and we thank the anonymous reviewers for their helpful comments.

References

Abaqus theory manual. 2019. Dassault Systèmes, Simulia Corp., Providence, Rhode Island, USA.

Abasolo, W., Eder, M., Yamauchi, K., Obel, N., Reinecke, A., Neumetzler, L., et al. 2009. Pectin may hinder the unfolding of xyloglucan chains during cell deformation: implications of the mechanical performance of *Arabidopsis* hypocotyls with pectin alterations. Mol. Plant, **2**(5): 990–999. doi:10.1093/mp/ssp065. PMID:19825674.

Arruda, E.M., and Boyce, M.C. 1993. A three-dimensional constitutive model for the large stretch behavior of rubber elastic materials. J. Mech. Phys. Solids, **41**(2): 389–412. doi:10.1016/0022-5096(93)90013-6.

ASTM. 2014. ASTM D638-14: standard test method for tensile properties of plastics. ASTM International, West Conshohocken, Penn.

Bergström, J.S. 2015. Mechanics of solid polymers: theory and computational modeling. William Andrew Publishing, Norwich, UK. doi:10.1016/C2013-0-15493-1.

Bidhendi, A.J., and Geitmann, A. 2016. Relating the mechanics of the primary plant cell wall to morphogenesis. J. Exp. Bot. **67**(2): 449–461. doi:10.1093/jxb/erv535. PMID:26689854.

Bidhendi, A.J., and Geitmann, A. 2018*a*. Finite element modeling of shape changes in plant cells. Plant Physiol. **176**(1): 41–56. doi:10.1104/pp.17.01684. PMID:29229695.

Bidhendi, A.J., and Geitmann, A. 2018*b*. Tensile testing of primary plant cells and tissues. *In* Plant biomechanics. *Edited by* A. Geitmann and J. Gril. Springer Cham. pp. 321–347. doi:10.1007/978-3-319-79099-2_15.

Bidhendi, A.J., and Geitmann, A. 2019. Methods to quantify primary plant cell wall mechanics. J. Exp. Bot. **70**(14): 3615–3648. doi:10.1093/jxb/erz281. PMID:31301141.

Bidhendi, A.J., Altartouri, B., Gosselin, F.P., and Geitmann, A. 2019. Mechanical stress initiates and sustains the morphogenesis of wavy leaf epidermal cells. Cell Rep. **28**: 1237–1250. doi:10.1016/j.celrep.2019.07.006.

Bolduc, J.-F., Lewis, L.J., Aubin, C.-É., and Geitmann, A. 2006. Finite-element analysis of geometrical factors in micro-indentation of pollen tubes. Biomech. Model. Mechanobiol. **5**(4): 227–236. doi:10.1007/s10237-005-0010-1. PMID:16514520.

Bou Daher, F., Chen, Y., Bozorg, B., Clough, J., Jönsson, H., and Braybrook, S.A. 2018. Anisotropic growth is achieved through the additive mechanical effect of material anisotropy and elastic asymmetry. eLife, **7**: e38161. doi:10.7554/eLife.38161. PMID:30226465.

Braybrook, S.A., and Peaucelle, A. 2013. Mechano-chemical aspects of organ formation in *Arabidopsis thaliana*: the relationship between auxin and pectin. PLoS ONE, **8**(3): e57813. doi:10.1371/journal.pone.0057813. PMID:23554870.

Carter, R., Woolfenden, H., Baillie, A., Amsbury, S., Carroll, S., Healicon, E., et al. 2017. Stomatal opening involves polar, not radial, stiffening of guard cells. Curr. Biol. **27**(19): 2974–2983. doi:10.1016/j.cub.2017.08.006. PMID:28943087.

Chagnon, G., Rebouah, M., and Favier, D. 2015. Hyperelastic energy densities for soft biological tissues: a review. J. Elast. **120**(2): 129–160. doi:10.1007/s10659-014-9508-z.

Chen, C.-C., Shih, W.-P., Chang, P.-Z., Lai, H.-M., Chang, S.-Y., Huang, P.-C., and Jeng, H. 2015. Onion artificial muscles. Appl. Phys. Lett. **106**(18): 183702. doi:10.1063/1.4917498.

Coats, B., and Margulies, S.S. 2006. Material properties of porcine parietal cortex. J. Biomech. **39**(13): 2521–2525. doi:10.1016/j.jbiomech.2005.07.020. PMID:16153652.

Cosgrove, D.J. 2005. Growth of the plant cell wall. Nat. Rev. Mol. Cell Biol. **6**(11): 850–861. doi:10.1038/nrm1746. PMID:16261190.

Cosgrove, D.J. 2015. Plant cell wall extensibility: connecting plant cell growth with cell wall structure, mechanics, and the action of wall-modifying enzymes. J. Exp. Bot. **67**(2): 463–476. doi:10.1093/jxb/erv511. PMID:26608646.

Cosgrove, D.J. 2018. Nanoscale structure, mechanics and growth of epidermal cell walls. Curr. Opin. Plant Biol. **46**: 77–86. doi:10.1016/j.pbi.2018.07.016. PMID:30142487.

Dorfmann, A., and Muhr, A. 1999. Constitutive models for rubber. A.A. Balkema, Rotterdam.

Fayant, P., Girlanda, O., Chebli, Y., Aubin, C.-É., Villemure, I., and Geitmann, A. 2010. Finite element model of polar growth in pollen tubes. Plant Cell, **22**(8): 2579–2593. doi:10.1105/tpc.110.075754. PMID:20699395.

Fung, Y. 1967. Elasticity of soft tissues in simple elongation. Am. J. Physiol. **213**(6): 1532–1544. doi:10.1152/ajplegacy.1967.213.6.1532. PMID:6075755.

Gasser, T.C., Ogden, R.W., and Holzapfel, G.A. 2005. Hyperelastic modelling of arterial layers with distributed collagen fibre orientations. J. R. Soc. Interface, **3**(6): 15–35. doi:10.1098/rsif.2005.0073. PMID:16849214.

Gooch, J.W. 2010. Encyclopedic dictionary of polymers. Springer New York, New York. pp. 729–729. doi:10.1007/978-1-4419-6247-8_11551.

Groves, R.B., Coulman, S., Birchall, J.C., and Evans, S.L. 2012. Quantifying the mechanical properties of human skin to optimise future microneedle device design. Comput. Methods Biomech. Biomed. Eng. **15**(1): 73–82. doi:10.1080/10255842.2011.596481.

Howard, J. 2014. Quantitative cell biology: the essential role of theory. Mol. Biol. Cell, **25**(22): 3438–3440. doi:10.1091/mbc.e14-02-0715. PMID:25368416.

Kierzkowski, D., Nakayama, N., Routier-Kierzkowska, A.-L., Weber, A., Bayer, E., Schorderet, M., et al. 2012. Elastic domains regulate growth and organogenesis in the plant shoot apical meristem. Science, **335**(6072): 1096–1099. doi:10.1126/science.1213100. PMID:22383847.

Kim, K., Yi, H., Zamil, M.S., Haque, M.A., and Puri, V.M. 2015. Multiscale stress–strain characterization of onion outer epidermal tissue in wet and dry states. Am. J. Bot. **102**(1): 12–20. doi:10.3732/ajb.1400273. PMID:25587144.

Lynch, T.M., and Lintilhac, P.M. 1997. Mechanical signals in plant development: a new method for single cell studies. Dev. Biol. **181**(2): 246–256. doi:10.1006/dbio.1996.8462. PMID:9013934.

Mihai, L.A., Budday, S., Holzapfel, G.A., Kuhl, E., and Goriely, A. 2017. A family of hyperelastic models for human brain tissue. J. Mech. Phys. Solids, **106**: 60–79. doi:10.1016/j.jmps.2017.05.015.

Milani, P., Braybrook, S.A., and Boudaoud, A. 2013. Shrinking the hammer: micromechanical approaches to morphogenesis. J. Exp. Bot. **64**(15): 4651–4662. doi:10.1093/jxb/ert169. PMID:23873995.

Morales-Orcajo, E., Souza, T.R., Bayod, J., and de Las, Casas, E.B. 2017. Non-linear finite element model to assess the effect of tendon forces on the foot–ankle complex. Med. Eng. Phys. **49**: 71–78. PMID:28807512.

Oey, M., Vanstreels, E., De Baerdemaeker, J., Tijskens, E., Ramon, H., Hertog, M., and Nicolai, B. 2007. Effect of turgor on micromechanical and structural properties of apple tissue: a quantitative analysis. Postharvest Biol. Technol. **44**(3): 240–247. doi:10.1016/j.postharvbio.2006.12.015.

Ogden, R.W. 1972. Large deformation isotropic elasticity — on the correlation of theory and experiment for incompressible rubberlike solids. Proc. Math. Phys. Eng. Sci. **326**(1567): 565–584. doi:10.1098/rspa.1972.0026.

Ogden, R.W. 1986. Recent advances in the phenomenological theory of rubber elasticity. Rubber Chem. Technol. **59**(3): 361–383. doi:10.5254/1.3538206.

Ogden, R., Saccomandi, G., and Sgura, I. 2004. Fitting hyperelastic models to experimental data. Comput. Mech. **34**(6): 484–502. doi:10.1007/s00466-004-0593-y.

Osorio, S., Castillejo, C., Quesada, M.A., Medina-Escobar, N., Brownsey, G.J., Suau, R., et al. 2008. Partial demethylation of oligogalacturonides by pectin methyl esterase 1 is required for eliciting defence responses in wild strawberry (*Fragaria vesca*). Plant J. **54**(1): 43–55. PMID:18088306.

Peaucelle, A., Wightman, R., and Höfte, H. 2015. The control of growth symmetry breaking in the *Arabidopsis* hypocotyl. Curr. Biol. **25**(13): 1746–1752. doi:10.1016/j.cub.2015.05.022. PMID:26073136.

Phyo, P., Wang, T., Kiemle, S.N., O'Neill, H., Pingali, S.V., Hong, M., and Cosgrove, D.J. 2017. Gradients in wall mechanics and polysaccharides along growing inflorescence stems. Plant Physiol. **175**(4): 1593–1607. doi:10.1104/pp.17.01270. PMID:29084904.

Remache, D., Caliez, M., Gratton, M., and Dos Santos, S. 2018. The effects of cyclic tensile and stress-relaxation tests on porcine skin. J. Mech. Behav. Biomed. Mater. **77**: 242–249. doi:10.1016/j.jmbbm.2017.09.009. PMID:28954243.

Robertson, D., and Cook, D. 2014. Unrealistic statistics: how average constitutive coefficients can produce non-physical results. J. Mech. Behav. Biomed. Mater. **40**: 234–239. doi:10.1016/j.jmbbm.2014.09.006. PMID:25247769.

Ryden, P., Sugimoto-Shirasu, K., Smith, A.C., Findlay, K., Reiter, W.D., and McCann, M.C. 2003. Tensile properties of *Arabidopsis* cell walls depend on both a xyloglucan cross-linked microfibrillar network and rhamnogalacturonan II-borate complexes. Plant Physiol. **132**(2): 1033–1040. doi:10.1104/pp.103.021873. PMID:12805631.

Sanati Nezhad, A., Naghavi, M., Packirisamy, M., Bhat, R., and Geitmann, A. 2013. Quantification of the Young's modulus of the primary plant cell wall using Bending-Lab-On-Chip (BLOC). Lab Chip, **13**(13): 2599–2608. doi:10.1039/c3lc00012e. PMID:23571308.

Sapala, A., Runions, A., Routier-Kierzkowska, A.-L., Gupta, M.D., Hong, L., Hofhuis, H., et al. 2018. Why plants make puzzle cells, and how their shape emerges. eLife, **7**: e32794. doi:10.7554/eLife.32794. PMID:29482719.

Savaldi-Goldstein, S., Peto, C., and Chory, J. 2007. The epidermis both drives and restricts plant shoot growth. Nature, **446**(7132): 199–202. doi:10.1038/nature05618. PMID:17344852.

Saxe, F., Weichold, S., Reinecke, A., Lisec, J., Döring, A., Neumetzler, L., et al. 2016. Age effects on hypocotyl mechanics. PLoS ONE, **11**(12): e0167808. doi:10.1371/journal.pone.0167808. PMID:27977698.

Shahzad, M., Kamran, A., Siddiqui, M.Z., and Farhan, M. 2015. Mechanical characterization and FE modelling of a hyperelastic material. Mater. Res. **18**(5): 918–924. doi:10.1590/1516-1439.320414.

Spatz, H., Kohler, L., and Niklas, K. 1999. Mechanical behaviour of plant tissues: composite materials or structures? J. Exp. Biol. **202**(23): 3269–3272. PMID:10562508.

Suslov, D., and Verbelen, J. 2006. Cellulose orientation determines mechanical anisotropy in onion epidermis cell walls. J. Exp. Bot. **57**(10): 2183–2192. doi:10.1093/jxb/erj177. PMID:16720609.

Suslov, D., Verbelen, J.-P., and Vissenberg, K. 2009. Onion epidermis as a new model to study the control of growth anisotropy in higher plants. J. Exp. Bot. **60**(14): 4175–4187. doi:10.1093/jxb/erp251. PMID:19684107.

Toole, G.A., Gunning, P.A., Parker, M.L., Smith, A.C., and Waldron, K.W. 2001. Fracture mechanics of the cell wall of *Chara corallina*. Planta, **212**(4): 606–611. doi:10.1007/s004250000425. PMID:11525518.

Van, Sandt, V.S., Suslov, D., Verbelen, J.-P., and Vissenberg, K. 2007. Xyloglucan endotransglucosylase activity loosens a plant cell wall. Ann. Bot. **100**(7): 1467–1473. doi:10.1093/aob/mcm248. PMID:17916584.

Vanstreels, E., Alamar, M., Verlinden, B., Enninghorst, A., Loodts, J., Tijskens, E., et al. 2005. Micromechanical behaviour of onion epidermal tissue. Postharvest Biol. Technol. **37**(2): 163–173. doi:10.1016/j.postharvbio.2005.04.004.

Wei, C., Lintilhac, P.M., and Tanguay, J.J. 2001. An insight into cell elasticity and load-bearing ability. Measurement and theory. Plant Physiol. **126**(3): 1129–1138. doi:10.1104/pp.126.3.1129. PMID:11457963.

Wei, C., Lintilhac, L.S., and Lintilhac, P.M. 2006. Loss of stability, pH, and the anisotropic extensibility of *Chara* cell walls.

Planta, **223**(5): 1058–1067. doi:10.1007/s00425-005-0152-5. PMID:16284777.

Yeoh, O.H. 1993. Some forms of the strain energy function for rubber. Rubber Chem. Technol. **66**(5): 754–771. doi:10.5254/1.3538343.

Yuan, S., Wu, Y., and Cosgrove, D.J. 2001. A fungal endoglucanase with plant cell wall extension activity. Plant Physiol. **127**(1): 324–333. doi:10.1104/pp.127.1.324. PMID:11553760.

Zamil, M.S., Yi, H., Haque, M., and Puri, V.M. 2013. Characterizing microscale biological samples under tensile loading: Stress–strain behavior of cell wall fragment of onion outer epidermis. Am. J. Bot. **100**(6): 1105–1115. doi:10.3732/ajb.1200649. PMID:23720433.

Zamil, M.S., Yi, H., and Puri, V.M. 2015. The mechanical properties of plant cell walls soft material at the subcellular scale: the implications of water and of the intercellular boundaries. J. Mater. Sci. **50**(20): 6608–6623. doi:10.1007/s10853-015-9204-9.

Zhang, T., Zheng, Y., and Cosgrove, D.J. 2016. Spatial organization of cellulose microfibrils and matrix polysaccharides in primary plant cell walls as imaged by multichannel atomic force microscopy. Plant J. **85**(2): 179–192. doi:10.1111/tpj.13102. PMID:26676644.

Zhu, M., Wang, Y., Zhu, S., Xu, L., Jia, C., Dai, J., et al. 2017. Anisotropic, transparent films with aligned cellulose nanofibers. Adv. Mater. **29**(21): 1606284. doi:10.1002/adma.201606284.